Calibration facility for solar wind plasma instrumentation

Adrian Marti, Reto Schletti, Peter Wurz,[a] and Peter Bochsler
Physikalisches Institut, University of Bern, CH-3012 Bern, Switzerland

(Received 12 April 2000; accepted for publication 13 November 2000)

Space-borne analysis of the composition of the solar wind offers the unique possibility of direct measurement of material originating from the sun. For development, testing, and calibration of solar wind particle instrumentation, particle beams of highly charged ions for all elements from hydrogen up to iron are needed. Although sources for these ions have been available for some time, the special demands of space instrumentation made it necessary to build a dedicated facility. We built an electron-cyclotron-resonance ion source operating at 2.45 GHz. The ion source is installed on a high voltage platform allowing for postacceleration potentials of up to 100 kV. Ions are produced from elements in gaseous and solid phase; the latter from vapor emitted from a high temperature furnace closely attached to the ion source. © *2001 American Institute of Physics.*
[DOI: 10.1063/1.1340020]

I. INTRODUCTION

The continuing interest in studying the solar wind composition and dynamics with space-borne instrumentation—some of the current missions are Ulysses,[1] WIND,[2] SOHO,[3] ACE[4]—has also stimulated the development of ever more sophisticated solar wind particle analyzers for future missions.[5] Typically, these instruments measure the mass per charge (m/q), the energy per charge, and the total energy for each ion detected in the particular field of view of the instrument. To derive physical parameters from these data, e.g., ion fluxes, densities, or temperatures, the transmission function of the employed instrument must be known as accurately as possible. The transmission function depends on several physical parameters of the incident ions such as direction, energy, and mass per charge of a species. Despite the availability of more and more powerful software packages to simulate ion-optical properties of instruments, experimental calibration of these instruments is still necessary to derive the transmission function. This is especially the case for isochronous time-of-flight spectrometers based on the carbon foil technique.[2–5]

Existing calibration facilities[6] for space plasma instrumentation are equipped with electron bombardment ion sources. These sources provide an excellent beam quality, however, for a limited set of gaseous ions and for low charge states[7] (at the required beam intensities) only. The calibration of a solar wind instrument requires a particle beam of highly charged ions for all elements from hydrogen up to iron (see Table I). Although sources for these ions have been available for some time,[8] the special demands of space instrumentation (beam current, purity, stability, availability of beam time, and instrument accommodation) motivated us to build a dedicated facility, which also alleviates many logistic problems encountered during external calibration campaigns.

For the first time, the new calibration facility allows the testing of plasma analyzers with beams of highly charged nonmetallic and metallic ions during all stages of instrument development. In addition, postlaunch calibrations of flight-spare instruments will allow improvement in knowledge of the transmission function of presently in-use instrumentation, and thus even improve the data analysis of already launched instruments.

The heart of the new calibration facility is an electron-cyclotron-resonance (ECR) ion source operating at 2.45 GHz using permanent magnets. This type of ion source allows the production of highly charged metallic and nonmetallic ions within the given constraints in power consumption and physical space available on our high voltage terminal. The ECR ion source is installed on this terminal to allow for postacceleration potentials of up to 100 kV to achieve solar wind-like energies. Ions are produced from elements in gaseous and solid phase, the latter from vapor emitted from a high temperature furnace closely attached to the ion source.

Calibration of sensors with metallic ions is important for the interpretation of solar wind data. Fractionation of the solar wind plasma occurring in the solar atmosphere is mainly attributed to the first ionization potential (FIP) of the elements.[9] Volatile elements provided by common calibration facilities are representative only for high FIP elements, whereas metallic elements in the solar wind all have a low FIP.

II. INSTRUMENTATION

A. Overview

The three main parts of the new calibration facility are the ECR ion source, the ion-optical system, and the main vacuum recipient (the experiment chamber) where the instrument to be tested is mounted (see Fig. 1).

The ECR ion source operates at a frequency of 2.45 GHz. The plasma is confined by a three-dimensional magnetic well established by permanent magnets. The design of this ion source is based on an earlier development at the University of Giessen,[10] which we adapted for our needs. Elements which are available in gaseous form at room tem-

[a]Electronic mail: wurz@soho.unibe.ch

TABLE I. Typical solar wind parameters at Earth orbit to be replicated by the calibration facility (from Refs. 19–23).

Element	Solar wind flux [$cm^{-2}\,s^{-1}$]	Solar wind charge state Range	Main energy range [keV]
H	2.5×10^{8}	1	0.5–3.5
He	9.7×10^{6}	2	2–14
O	1.3×10^{5}	6–8	8–57
Fe	1.2×10^{4}	7–16	28–200
Ca	2.0×10^{3}	8–12	20–140
Ar	5.5×10^{2}	8–12	20–140

perature are directly introduced into the ion source via a proportional integral derivative (PID) regulated piezovalve, which allows the plasma discharge to be maintained at a constant gas pressure even if the line pressure from the gas supplies drops significantly during long runs of the ion source. To allow the production of metallic ions, we added a high temperature furnace with its opening facing the central zone of the ion source where the plasma is burning. From this central zone, the ions are extracted by lifting the potential of the ion source including the high temperature furnace to a potential of maximum 10 kV with respect to the following beam line. A mechanically adjustable extraction electrode system allows the optimization of the electric field in the space-charge-limited region of the initial ion acceleration for a particular m/q.

As shown in Fig. 2, the ion-optical system is comprised of an Einzel lens, a set of deflection plates, a Wien filter, a 180° hemispherical energy per charge analyzer, a second Einzel lens, and a drift tube which transmits the ions through the exit aperture into the main vacuum chamber. The ECR ion source with the accompanying ion-optical elements is installed on a high voltage platform allowing for postacceleration potentials of up to 100 kV. After passing the high voltage insulator, located after the exit aperture, the ions enter the vacuum recipient where the instrument to be tested is placed (see Fig. 1). A beam scanning system equipped with a Faraday cup and a channeltron allows measurement of the spatial intensity distribution of the ion beam. Furthermore, together with the Wien filter, the ion current measurement with the beams scanner is used to select an appropriate m/q in the ion beam.

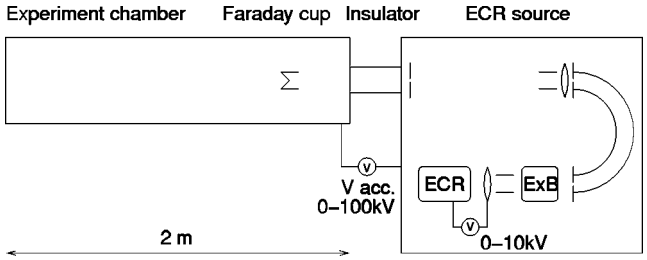

FIG. 1. Schematics of the ECR ion source, of the ion-optical system, and of the experiment chamber. The source is mounted on a high voltage terminal, which allows for acceleration of the beam of up to 100 keV per charge. Instruments to be calibrated are mounted into the experiment chamber.

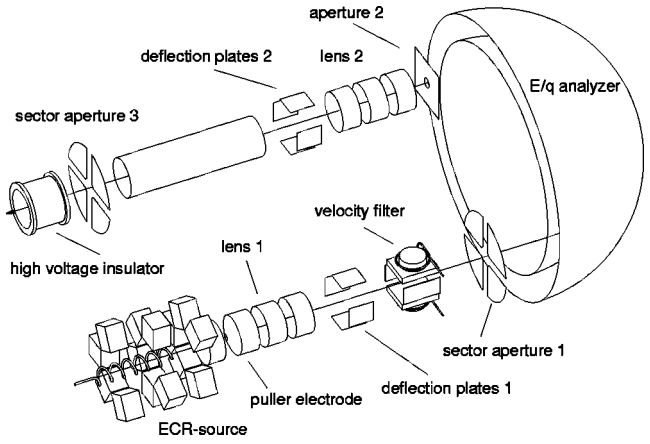

FIG. 2. Detailed schematics of the ECR ion source and of the ion-optical system. Few permanent magnets have been removed from the drawing to give sight of the volume where the ECR process happens. The ions are extracted by the puller electrode with a potential of up to 10 kV. With the first Einzel lens (lens 1) and deflection plates 1 the beam can be focused onto the entrance aperture of the hemispherical E/q analyzer. On their way the ions pass a velocity filter where a m/q filtering takes place. After the E/q analyzer the beam is reshaped by the second Einzel lens (lens 2) and the second set of deflection plates before it leaves the source chamber into the experiment chamber (not shown on this drawing) after being accelerated in the high voltage insulator with a potential of up to 100 kV. The length of the system is about 1.2 m.

B. Ion source

The principle of the ECR ion source has already been described in detail elsewhere.[10,11] The magnetic bottle confining the plasma is built entirely from permanent magnets. The 18 Fe–Nd–B magnetic blocks have a dimension of 65 $\times52\times36.6$ mm^3 and are arranged in three rings of six blocks each. The minimum B structure is obtained by superposition of an axial and a radial magnetic field. The direction of magnetization of the blocks of the first ring is chosen to point toward the axis while the blocks of the third ring point toward the opposite direction (see Fig. 3). This arrangement produces the axial B field between the two rings pointing along the beam extraction direction with a minimum centered between the two rings (see Fig. 4). Iron plates installed between the magnetic rings help to increase the mirror ratio r_m defined and measured[10] as

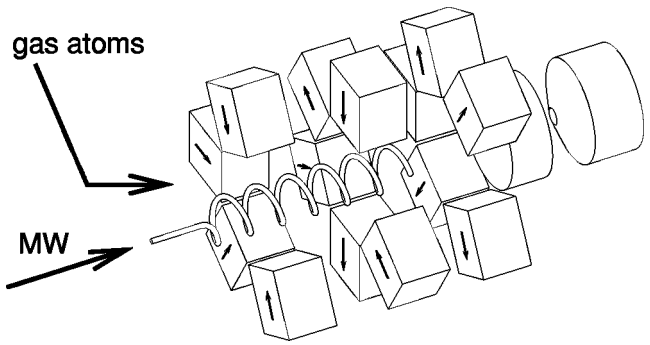

FIG. 3. Schematics of the ECR source. The orientation of the magnetization of the permanent magnets, which are responsible for the minimum B structure, is indicated with arrows on each individual block. Few of the 18 blocks have been omitted in the drawing to allow view into the plasma region. The microwave (MW) is radiated into the plasma tube with a helix antenna.

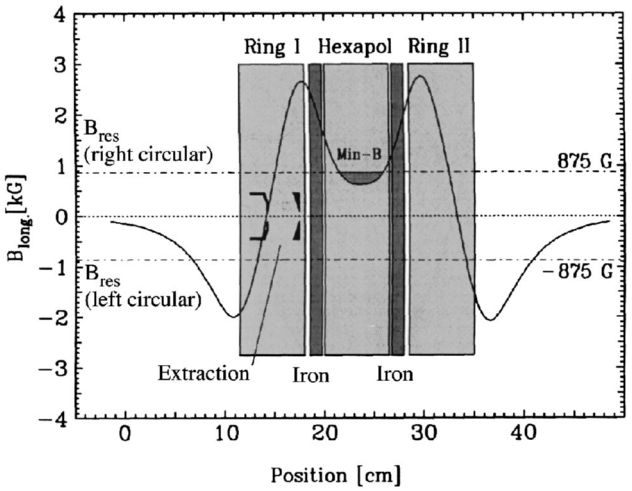

FIG. 4. Magnetic field strength and minimum B structure in the source. Reproduced from Ref. 24.

$$r_m = \frac{B_{\max}}{B_{\min}} \simeq \frac{240\,\mathrm{mT}}{60\,\mathrm{mT}} = 4. \tag{1}$$

The second ring, arranged to form a hexapolar field (alternating direction of the magnetization of the six blocks), produces the radial component of the *B* field for the three-dimensional well in the center of the ECR source. The use of permanent magnets and the absence of electric coils allows a substantial reduction of the electrical power consumption of the ion source. Since the ECR ion source is installed on a 100 kV high voltage terminal, this results in a significant simplification of the electric power equipment.

The principle of the ECR source is as follows: The electrons confined in the minimum *B* structure are first heated resonantly by circular-polarized microwave radiation with the frequency of the electron-cyclotron resonance (2.45 GHz) along the 0.0875 T contour of the magnetic field. Then, the atoms are ionized by collisions with the hot electron plasma. The confinement time of the ions in the source region is sufficient to undergo multiple collisions with the electrons, resulting in sequential ionization into higher charge states. The ions then leave the source through the loss cone of the magnetic bottle. For typical operating conditions, the resonant heating leads to electron temperatures around 1 MK with suprathermal non-Maxwellian tails at higher energies. The electron temperature has been estimated from the measured charge state distribution.[12]

The microwave system consists of a 2.45 GHz continuous wave magnetron (Muegge, model MW 46 009) with a maximal power of 300 W, a waveguide (R26), a Teflon HV insulator to separate the ion source and the microwave system galvanically, a crossbar adapter to couple the microwave from the waveguide to a coaxial line, and finally a helix antenna to provide a circular polarized alternating field. A circulator with an absorber (Philips, 2 kW) is included in the system to avoid damage of the magnetron by reflected waves. A tuner with a threefold of variable shorts in the waveguide is used to adapt to the impedance of the plasma and therefore to optimize the electron heating.

The electric potential of the ion source can be lifted to a potential U_0 of up to 10 kV with respect to the high voltage terminal to extract the ions from the ECR source. This makes the insertion of additional insulators into the gas inlet system, the waveguide, and the vacuum enclosure of the ion path necessary. The gas inlet system is equipped with a gas manifold of five inlet valves to connect standardized laboratory gas bottles of 1 *l* volume. The gas pressure is automatically controlled by a PID regulated piezoelectric valve (PCS01, von Ardenne GmbH). To allow the production of metallic ions, we added a high temperature furnace (high temperature effusion cell: HTEZ, MBE–Komponenten GmbH) with its opening facing the central zone of the ion source at the location of the plasma (see Fig. 5). Neutral vapor released from the furnace drifts through the magnetic enclosure directly into the ion source. The atoms of the vapor are ionized by the electrons of an auxiliary plasma (typically H_2 or He) burning in the source.

With furnace temperatures of up to 2000 °C all elements observed in the solar wind can be generated with this facility.

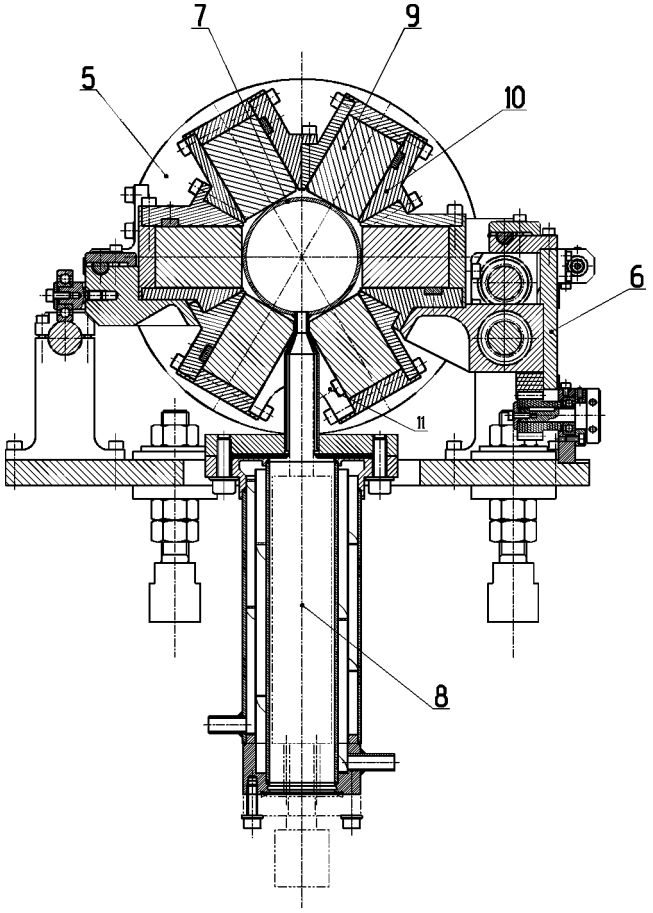

FIG. 5. Cross section of the ECR source and of the high temperature furnace. The minimum *B* structure is obtained with a special configuration of the permanent magnets (9) arranged in three rings and separated with two iron plates (5). The magnets are held together with a set of bronze insets (10) around the plasma tube (7). The whole source is held on a carriage (6) movable along the plasma tube axis. The high temperature furnace (dashed line) is placed from the bottom into the cooling mantle (8). This allows for a rapid change of the furnace load. Evaporated metal atoms can drift directly into the plasma tube to be ionized there.

C. Ion optical elements

The schematics of the arrangement of the ion optical elements are shown in Fig. 2. To extract the ions from the ion source, a high voltage U_0 of up to 10 kV is applied between the extraction electrode of the plasma chamber and the following puller electrode. To gain maximum flexibility for optimizing the ion beam, the extraction potential as well as the distance between the two electrodes can be varied, the latter from 1.5 to 17.5 mm. The first electrostatic Einzel lens is directly mounted behind the puller electrode and has an inner diameter of 46 mm. The two Einzel lens assemblies consist of three cylindrical lens elements each of 50 mm length and 46 mm inner diameter, followed by two pairs of 80-mm-long deflector plates. The gap between two cylindrical elements is 5 mm. To avoid field distorting oxide layers on the electrodes, we made all ion-optical elements completely out of pyrolytic graphite (le Carbone No. 2114). The Einzel lens assembly is electrically isolated and mounted on eight polished aligned metal rods along the outside perimeter of the lens assembly. These metal rods also supply the various electrical potentials to the lens elements and return the current collected on these elements. Electrical contacts are made of copper–beryllium springs located between the rods and the lens elements.

The Wien filter (model 600-B, Colutron Research Corporation) is located after the first Einzel lens. An ion passes straight through the velocity filter ($E\times B$ filter) if the Coulomb force of the E field is balanced by the Lorenz force of the B field. This is the case for an ion if

$$\frac{m}{q}=2\,U_0\frac{B^2}{E^2}, \tag{2}$$

with U_0 being the acceleration voltage. This allows for separation of the different ion species by their mass per charge m/q. The maximal E field is $E_{\max}=16.8$ kV/m and the maximal B field is $B_{\max}=0.3$ T.

The ion-optical transmission of the system has to be optimized for measurements at high charge states, where the current densities are low. This implies a limitation of the mass resolution $m/\Delta m$. Good results have been obtained for $m/\Delta m\simeq 14$ (see Sec. III). The three apertures in the beam line are all 8 mm in diameter, including the final m/q selecting aperture. Simultaneously, this allowed us to keep the ratio of backscattered ions at the exit of the velocity filter as low as possible and so to reduce the contamination of the insulating elements within the filter.

The radii of the inner and the outer hemispheres of the E/q analyzer are $R_1=116.4$ mm and $R_2=135$ mm, respectively. The nominal ion path is at $R_n=125$ mm and the analyzer constant k is 6.76. Ultraviolet (UV) light produced within the ECR source has to be suppressed since microchannel plate detectors, often used in space instrumentation, are UV sensitive. A photon needs to be scattered at least four times to transit the E/q analyzer due to the narrow gap between the inner and the outer hemisphere. To maximize UV suppression, the two hemispheres are made entirely out of graphite. The surfaces exposed to the ion beam are sand blasted with fine-grained sand to increase their roughness on the length scale of $<\mu$m to maximize absorption and diffuse reflection of the unwanted UV photons.[13] An overall UV suppression of 4×10^{25} is reached[11] assuming isotropic Lambert scattering. The count rate due to photons measured with the channeltron of the beam monitor (5 mm aperture) is about 0.2 Hz during operation of the ECR source.

D. Beam diagnostics

Three current-measuring apertures are placed at key places along the beam path at intermediate ion-optical focal points (see Fig. 2). They provide the capability for optimizing the settings of the various ion-optical subsystems and allow a continuous monitoring of the beam. Two of these apertures are segmented into four sectors to obtain information on the alignment of the ion beam with respect to the ion-optical axis. The currents collected on the apertures are logarithmically amplified and displayed on ten-element light emitting diode (LED)-bar displays covering a current range from 1 nA to 1 mA. These LED bars provide good qualitative information, which is used primarily during the initial setup of the beam line.

The beam monitor, located in the main vacuum chamber, consists of two detectors: a channeltron detector and a Faraday cup detector. Both detectors are mounted on a lever arm, which can be moved over the two-dimensional area of the ion beam (see Fig. 6). The pendulum-like moving pattern of the beam monitor is controlled by two stepping motors located outside of the vacuum chamber. It was the aim of this design to avoid any movable parts within the vacuum. A vacuum-tight bellows acts as the mechanical connection between the vacuum chamber and the movable arm. Control of the stepping motors as well as signal readout of the detectors is facilitated by a laboratory computer.

The channeltron can be operated in pulse counting or continuous mode using a transimpedance amplifier. The special shape of the inner electrode of the Faraday cup in combination with an entrance aperture minimizes the flux of backscattered secondary electrons and secondary ions. The Faraday cup is used for absolute current measurements to determine instrument efficiencies and also to calibrate the channeltron. The Faraday cup has the same active area as the channeltron which can be varied selecting one of five available apertures with diameters ranging from 1 to 5 mm without breaking the vacuum. Ion currents as low as 10^{-13} A can be measured with this Faraday cup.

The beam monitor can be used to examine the shape of the ion beam. Figure 7 shows a typical beam profile recorded on a quadratic grid perpendicular to the ion-optical axis. Quicker results can be obtained by recording only horizontal and vertical intensity profiles. To examine the charge state distribution within an ion beam, the beam monitor is fixed at its center position. An appropriate variation of the current of the magnetic coils of the Wien filter allows us to acquire the beam intensity as a function of mass per charge ratio according to Eq. (2). Charge state distributions are shown in Sec. III B.

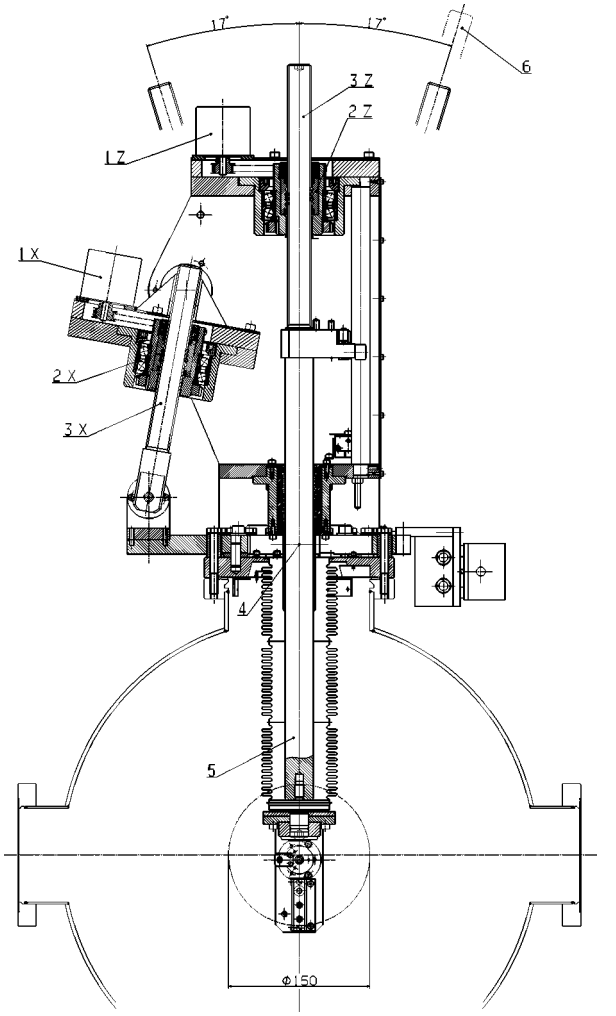

FIG. 6. Cross section of the experiment chamber at the beam monitor position. The Faraday cup and the channeltron (in the circle) can be moved along the axis of the lever arm (5) and rotated about the axis located at (4). Two stepping motors control the motion. All mechanical parts are outside of the vacuum chamber. For measurements, with an experiment positioned downstream of the beam, the beam monitor has to be parked in a position near one of the two windows.

E. Experiment chamber

Acceleration of the ion beam is possible to energies of up to 100 keV per charge. A stack of 20 metal rings at high voltages, supplied from a voltage divider, form a homogeneous accelerating E field. It is placed inside a ceramic insulator of ~200 mm length and 153.3 mm inner diameter, located between the inner and outer Faraday cage of the ion source assembly. Grids are mounted on the first and on the last ring of the stack to avoid field distortion. The ions of the desired charge state and velocity enter the experiment chamber which contains the beam monitor and the instrument to be examined. The chamber is a tube of 2 m length and of 0.5 m diameter, allowing exposure of complete instruments including their entrance systems to the ion beam. A laser beam is aligned with the ion beam axis and gives the necessary positioning information for placing the instruments to be calibrated. The ion source chamber and the experimental chamber can be separated by a gate valve into two autonomous vacuum units; each is equipped with its own turbomolecular pumping system and vacuum control. This gives maximum flexibility for installation of instruments into the experiment chamber and for maintenance of the ion source assembly. Independent vacuum lines reduce pumping time and down time of the facility. A vacuum protection circuit is set up in both chambers to automatically turn off all power connected to it (e.g., HV supplies) once the pressure in the chamber exceeds a preset value. The experiment chamber is equipped with two baking out systems (thermal and ultraviolet lamp) to reduce residual gas pressure and pumping time. A quadrupole mass spectrometer is also available to analyze the composition of the residual gas. The lowest obtainable pressure in the experiment chamber is in the low 10^{-8} mbar range.

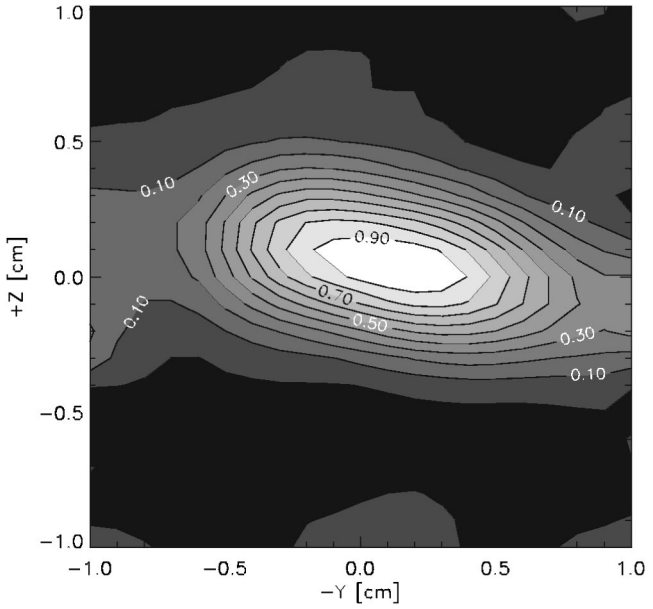

FIG. 7. Beam profile at the position of the beam diagnostic system inside the experimental chamber. The contour lines indicate the beam intensity in the $(-Y,+Z)$ plane, normal to the beam axis in direction of the beam. The maximum current density was 0.12 pA mm^{-2} for this selected 18 keV O^{3+} beam.

III. PERFORMANCE

A. Beam profile

In a first step we optimized the position of the magnetic bottle and of the extraction electrodes according to Refs. 14–16. Simultaneously, we maximized the ion current and focused the extracted beam as tightly as possible. Figure 7 shows a typical pattern of a 18 keV O^{3+} ion beam acquired with the beam monitor. The current was measured with the Faraday cup using the 5-mm-diam aperture on a 21×21 grid, spanning an area of 4 cm^2. The total current measured was 6.3 pA. The maximal current density was 0.12 pA mm^{-2}, which corresponds to a particle flux of 2.5×10^5 s^{-1} mm^{-2}. The beam width along the two principal axes was 11.7 and 4.2 mm full width at half maximum, respectively.

B. Charge states

The analysis of different charge states in the ion beam is performed with the Wien filter. To prevent beam distortions

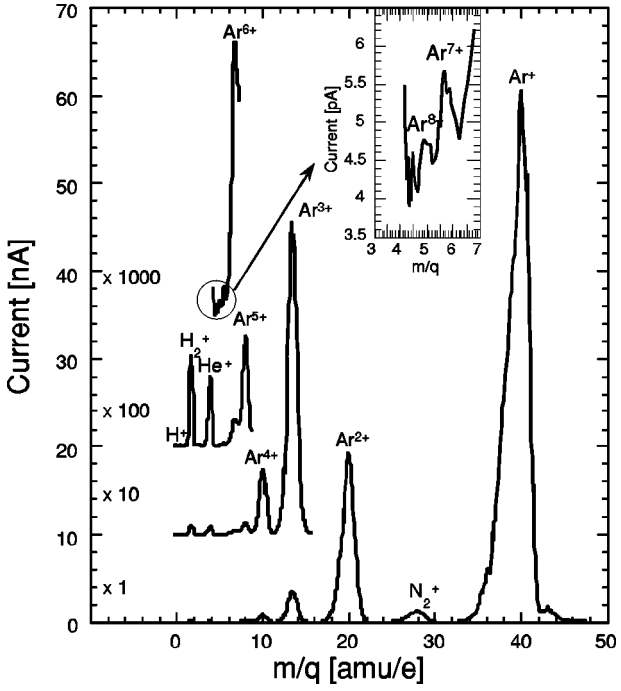

FIG. 8. Charge state distribution of an argon ion beam.

by the velocity filter, the potentials of its electrode stacks[17] had to be carefully balanced out. For these adjustments we used helium because it provides high beam currents and produces a simple charge state distribution.

1. Nonmetallic ions

To determine the performance of the ion source we first used argon. With the Faraday cup (5 mm aperture), we were able to detect from singly up to sixfold charged argon in the ion beam with beam currents varying from 60 nA (Ar^+) to 30 pA (Ar^{6+}). With the channeltron, the higher charge states Ar^{7+} and Ar^{8+} were detected, with ion currents of 1 and 0.5 pA, respectively. The measured ion currents as a function of their m/q ratio are shown in Fig. 8. Contributions from the residual gas can be seen: at $m/q=28$ from N_2^+, at $m/q=4$ from He^+, at $m/q=2$ from He^{2+} and H_2^+, and at $m/q=1$ from H^+. Another measurement with oxygen at higher mass resolution $m/\Delta m \simeq 30$ is shown in Fig. 9. The current for O^+ was 10 nA. A small peak at $m/q=3.2$, identified as O^{5+}, was present in the spectrum. O^{4+} was partly hidden by the helium peak from the residual gas. Other contributions from the residual gas (caused by a tiny air leak) are found in the spectrum at different charge states. These ions are debris of molecules like N_2, O_2, H_2O, and CO_2. The dynamic range of the spectrum spans five orders of magnitude.

2. Metallic ions

For the production of metallic ions with the high temperature furnace, an auxiliary plasma has to be maintained for a stable ECR ionization process. For example, helium has been suggested by others[18] because of the high electron densities and high beam stability achieved. Hydrogen is another gas we use for the auxiliary plasma to alleviate interferences

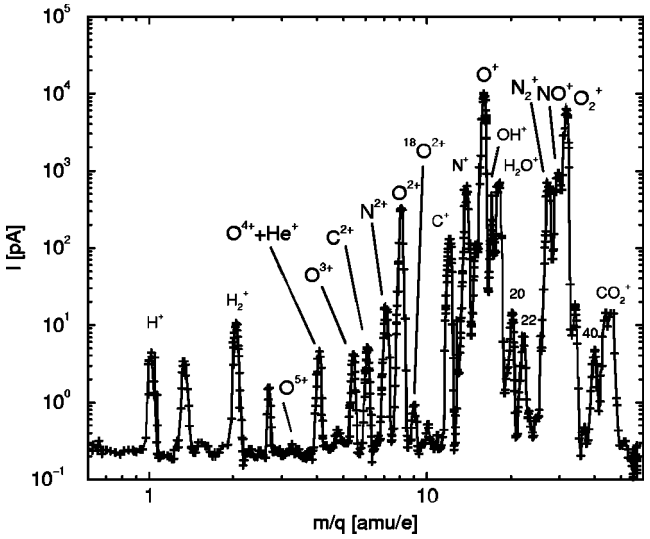

FIG. 9. Spectrum of an oxygen beam at higher m/q resolution.

in m/q. Neutral metal atoms stream from the high temperature furnace (see Fig. 5) into the ECR zone where they penetrate the auxiliary plasma. The metallic ions captured in the minimum B structure are ionized in steps up to higher charge states due to collisions with the hot electrons. The extracted ion beam is composed of metallic ions as well as ions from the auxiliary plasma. For a first test run, a calcium rod (purity 99.9%, length 10 mm, radius 4 mm) was loaded into the furnace using a pyrolytic boron nitride crucible. The temperature was stepwise increased up to 470 °C due to heavy gas load from outgassing. We could measure 0.4 nA of Ca^+ with the Faraday cup (5 mm aperture). The complete charge

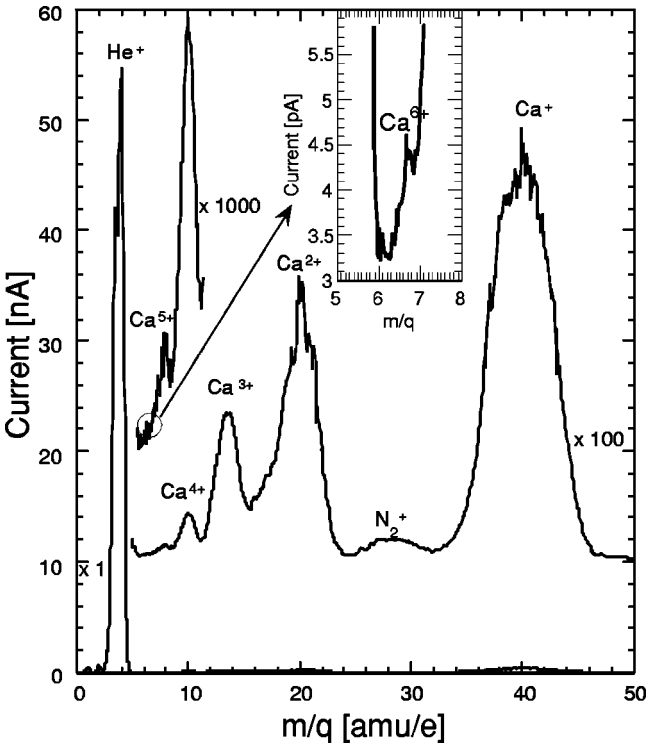

FIG. 10. Charge state distribution of a calcium beam. A solid calcium rod was heated in the high temperature furnace to 470 °C to evaporate Ca into the auxiliary helium plasma.

TABLE II. Fluxes and charge states obtained with the ECR source.

Element	Particle flux range $[cm^{-2}\,s^{-1}]$	Charge state range
O	3.1×10^{11}–5×10^{5}	1–5
Ca	1.2×10^{10}–2.3×10^{7}	1–6
Ar	1.8×10^{12}–3×10^{6}	1–8

state distribution is shown in Fig. 10. Ca^{2+} up to Ca^{6+} have been detected with ion currents ranging from 260 to 0.5 pA. Higher charge states, Ca^{7+}–Ca^{10+} are hidden below the prominent He^{+} signal of 55 nA from the auxiliary plasma.

From the charge state distribution of Ar ions and Ca ions, the electron density $n_e=5\times10^{9}$ cm^{-3}, the confinement time $t_c=10^{-3}$ s, and the electron temperature $T_e=100$ eV can be inferred.[12] The degree of ionization is of the order of 10%.

C. Beam stability

The ion current of an Ar^{4+} beam remained at 0.29 ± 0.01 nA for up to 5 h without any readjustments, and during a 48 h continuous run, the Ar^{4+} beam remained at 0.26 ± 0.03 nA. The 18 cm^3 gas reservoir was refilled three times during this run. No other manipulation was necessary.

D. Discussion

High charge states for a broad range of species, a wide energy range, and beam stability are crucial parameters of a calibration facility for space plasma spectrometers. The energy range and the beam stability of the facility meet these requirements. Table II summarizes the measured particle flux and charge state ranges. A comparison with Table I shows that the flux range is high enough even for the high charge states. Even though the achieved charge state range does not cover the solar wind range, an expanded range is available compared to existing facilities. Together with the availability of metallic ions, the new calibration chamber will extend the scope of available calibration data for space plasma instrumentation. Further enhancements to the source and an upgrade of the experiment chamber similar to actual calibration facilities, including the possibility of shifting and rotating instruments within the chamber and to provide full automated measurements, are planned for the future.

ACKNOWLEDGMENTS

The authors are grateful to J. Fischer, H. Hofstetter, and R. Liniger, from the University of Bern, for their contributions in the areas of design, fabrication, and electronics, respectively, and to E. Salzborn, R. Trassl, and M. Liehr from the University of Giessen, Germany. This work is supported by the Swiss National Foundation.

[1] K.-P. Wenzel, R. G. Marsden, D. E. Page, and E. J. Smith, Astron. Astrophys., Suppl. Ser. **2**, 207 (1992).
[2] G. Gloeckler, H. Balsiger, A. Bürgi, P. Bochsler, L. A. Fisk, A. B. Galvin, J. Geiss, F. Gliem, D. C. Hamilton, T. E. Holzer, D. Hovestadt, F. M. Ipavich, E. Kirsch, R. A. Lundgren, K. W. Ogilvie, R. B. Sheldon, and B. Wilken, Space Sci. Rev. **71**, 79 (1995).
[3] D. Hovestadt, M. Hilchenbach, A. Bürgi, B. Klecker, P. Laeverenz, M. Scholer, H. Grünwaldt, W. I. Axford, S. Livi, E. Marsch, B. Wilken, P. Winterhoff, F. M. Ipavich, P. Bedini, M. A. Coplan, A. B. Galvin, G. Gloeckler, P. Bochsler, H. Balsiger, J. Fischer , J. Geiss, R. Kallenbach, P. Wurz, K. U. Reiche, F. Gliem, D. L. Judge, K. C. Hsieh, E. Moebius, M. A. Lee, G. G. Managadze, M. I. Verigin, and M. Neugebauer, Sol. Phys. **162**, 441 (1995).
[4] G. Gloeckler, J. Cain, F. M. Ipavich, E. O. Tums, P. Bedini, L. A. Fisk, T. H. Zurbuchen, P. Bochsler, J. Fischer, R. F. Wimmer-Schweingruber, J. Geiss, and R. Kallenbach, Space Sci. Rev. **86**, 497 (1998).
[5] P. Wurz, L. Gubler, P. Bochsler, and E. Moebius, in *Measurement Techniques in Space Plasmas: Particles*, Vol. 102 of *American Geophysical Monograph*, edited by R. F. Pfaff, J. E. Borovsky, and D. T. Young (American Geophysical Union, Washington, DC, 1998), pp. 229–235.
[6] M. Steinacher, F. Jost, and U. Schwab, Rev. Sci. Instrum. **66**, 4180 (1995).
[7] A. G. Ghielmetti, H. Balsiger, R. Baenninger, P. Eberhardt, J. Geiss, and D. T. Young, Rev. Sci. Instrum. **54**, 425 (1983).
[8] R. Geller, *Electron Cyclotron Resonance Ion Sources and ECR Plasmas* (Institute of Physics, Bristol, 1996).
[9] U. Feldman, Phys. Scr. **46**, 202 (1992).
[10] M. Liehr, R. Trassl, M. Schlapp, and E. Salzborn, Rev. Sci. Instrum. **63**, 2541 (1992).
[11] A. Marti, Ph.D. thesis, University of Bern, Switzerland, 1997.
[12] P. Wurz, A. Marti, and P. Bochsler, Helv. Phys. Acta **71**, 23 (1998).
[13] T. Zurbuchen, P. Bochsler, and F. Scholze, Opt. Eng. (Bellingham) **34**, 1303 (1994).
[14] S. Fiedler, Master's thesis, Technische Universität Wien, 1991.
[15] M. Lietner, Master's thesis, Institut für Allgemeine Physik, Technische Universität Wien, Austria, 1993.
[16] G. Evers, Master's thesis, Institut für Kernphysik, Strahlenzentrum der Justus-Liebig-Universität Giessen, 1995.
[17] L. Wåhlin, Nucl. Instrum. Methods **27**, 55 (1964).
[18] L. Bex, M. P. Bourgarel, P. Sortais, P. Attal, M. Bisch, P. Leherissier, J. Y. Pacquet, and Y. Bourgoin, NSCL Report No. MSUCP-47, National Superconducting Laboratory, 5027-14021 Caen Cedex, France.
[19] A. B. Galvin, F. M. Ipavich, C. M. S. Cohen, G. Gloeckler, and R. von Steiger, Space Sci. Rev. **72**, 65 (1995).
[20] M. R. Aellig, S. Hefti, H. Grünwaldt, P. Bochsler, P. Wurz, F. M. Ipavich, and D. Hovestadt, J. Geophys. Res., [Space Phys.] **104**, 24769 (1999).
[21] G. Gloeckler and J. Geiss, AIP Conf. Proc. **183**, 49 (1989).
[22] Y. Ko, G. Gloeckler, C. M. S. Cohen, and A. B. Galvin, J. Geophys. Res., [Space Phys.] **104**, 17005 (1999).
[23] O. Kern, Ph.D. thesis, University of Bern, 1999.
[24] M. Liehr, Ph.D. thesis, University of Giessen, Germany, 1992.